Supplementary materials

for

Effects of crosslinking position and degree of conjugated microporous polymers based on perylene tetraanhydride bisimide on the fluorescence sensing performance

Chen Hu[a], Ying-Chun Gao[a], Can Zhang[a], Min Liu[a], and Tong-Mou Geng[a]*

a AnHui Province Key Laboratory of Optoelectronic and Magnetism Functional Materials; School of Chemistry and Chemical Engineering, Anqing Normal University, Anqing 246011, China

Corresponding Author:

Tongmou Geng

Mailing Address: School of Chemistry and Chemical Engineering, Anqing Normal University, Anqing 246011, China

E-mail addresses: gengtongmou@aqnu.edu.cn (TM Geng).

Synthesis of DP_4A_0 and DP_4A_2

The DP_4A_0 was synthesized by Sonogashira-Hagihara cross coupling condensation reaction of arylhalides and arylethynylenes. In a typical procedure, 1,4-diethynylbenzene (DEB) (0.1892 g, 1.5 mmol), PBr_4ABr_0 (0.8581 g, 1 mmol), tetrakis-(triphenylphosphine) palladium(0) (40 mg, 0.0334 mmol) and copper(I) iodide (20 mg, 0.10 mmol) were placed in a dry 50 mL flask. The solids were dissolved in a mixture of anhydrous N-N-dimethylformamide (DMF) (8 mL) and anhydrous diisopropylamine (DIA) (8 mL). After the reaction mixture was degassed, the flask was placed in oil bath at 90 ^oC and stirred for 3 days. The solid product was then collected by filtration and washed well with chloroform, water, acetone and methanol each for four times (4×20 mL). Then, the solid was further washed with chloroform for 24 h, and methanol for 24 h using a Soxhlet extractor. The solid was dried at 50 ^oC in a vacuum oven for 24 h to afford black powder (1.0363 g, 99 %). Solid state CP/MAS ^{13}C NMR (δ ppm): 161.52 (C=O), 146.93 (ϕ), 128.18, 122.23 (ϕ), 93.40 (-C≡C-), 82.83, 77.87 (≡C-H). FT-IR (KBr, cm^{-1}): 3415 (ν_{H2O}); 3047 ($\nu_{\phi\text{-}H}$); 2189 ($\nu_{C\equiv C\text{-}}$); 1709, 1666 (perylene carboxylic acid bisimine characteristic peak); 1591, 1485, 1405 ($\nu_{C=C}$); 1331 ($\nu_{C\text{-}N}$); 744, 696 (ϕ-H, mono substituted benzene C-H out of plane deformation absorption peak). Anal. calcd. for $C_{56}H_{26}O_4N_2$ (790.80): C 85.05, H 3.31, N 3.54; found: C 77.65, H 3.645, N 3.934.

DP_4A_2 was synthesized using the similar procedures as described for DP_4A_0. PBr_4ABr_2 (0.6792 g, 0.6667 mmol) was used. DP_4A_2 was obtained as a black powder (0.8693 g, yield: 95.01 %). Solid state CP/MAS ^{13}C NMR (δ ppm): 161.86 (C=O),

130.81 (ϕ), 122.03 (ϕ), 90.97 (-C≡C-), 83.05, 77.64 (≡C-H). FT-IR (KBr, cm^{-1}): 3415 (ν_{H2O}); 3031 ($\nu_{\phi\text{-}H}$); 2200 ($\nu_{C\equiv C\text{-}}$); 1714, 1667 (perylene carboxylic acid bisimine characteristic peak); 1591, 1501, 1405 ($\nu_{C=C}$); 1335 ($\nu_{C\text{-}N}$); 755, 546 (ϕ-H, mono substituted benzene C-H out of plane deformation absorption peak). Anal. calcd. for $C_{66}H_{30}O_4N_2$ (914.96): C 86.64, H 3.30, N 3.06; found: C 72.77, H 3.395, N 4.034.

Preparation, characterization, morphology analysis, pore performance, and fluorescent sensing performance of DP_2A_2 refer to refs [14].

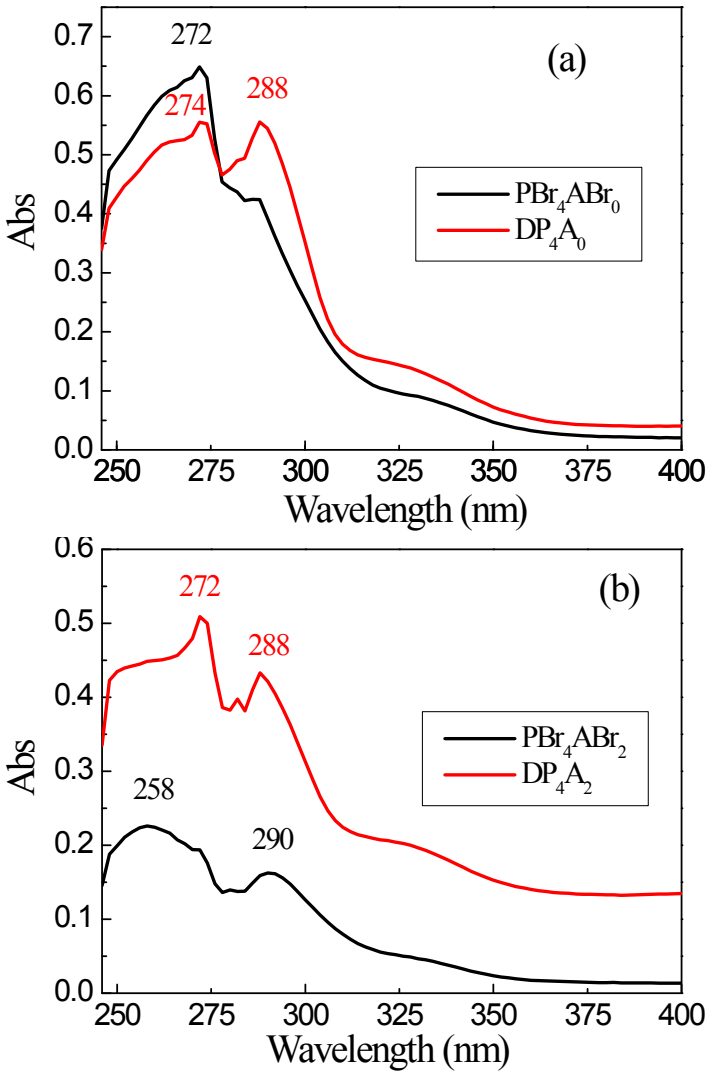

Fig. S1 The solid UV−vis absorption spectra of the (a) PBr_4ABr_0, DP_4A_0, and (b) PBr_4ABr_2, DP_4A_2.

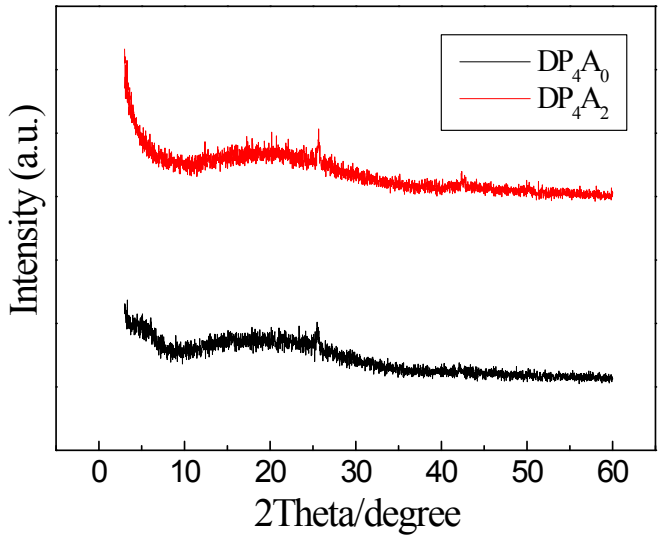

Fig. S2 X-ray powder diffraction patterns of DP_4A_0 and DP_4A_2.

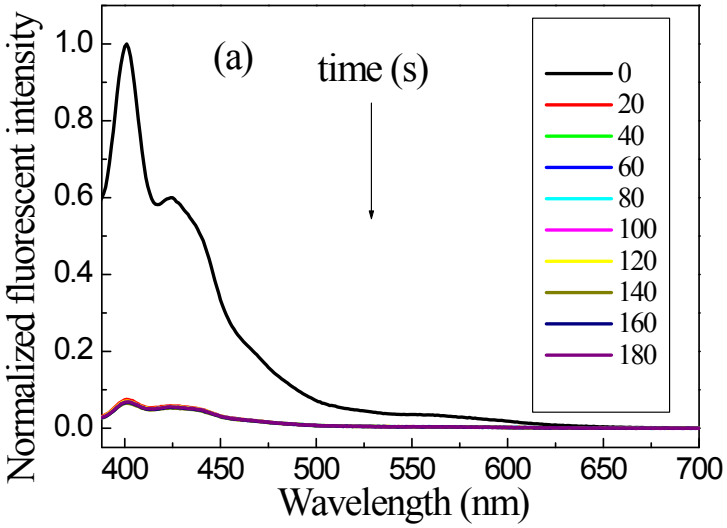

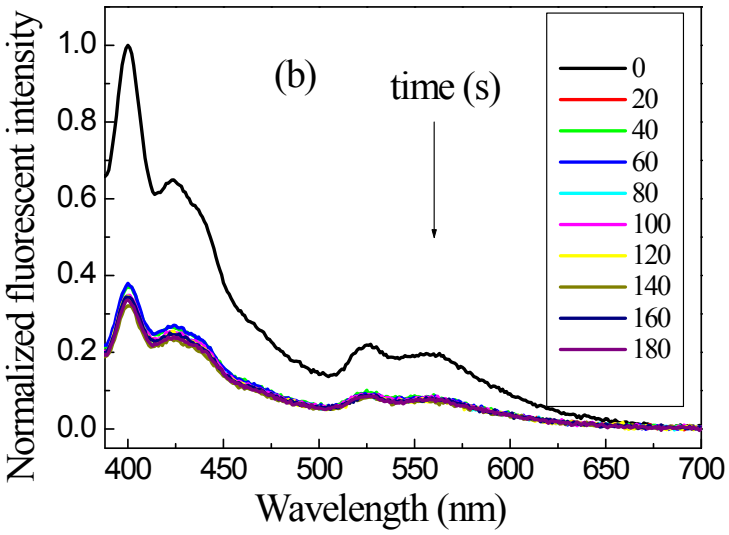

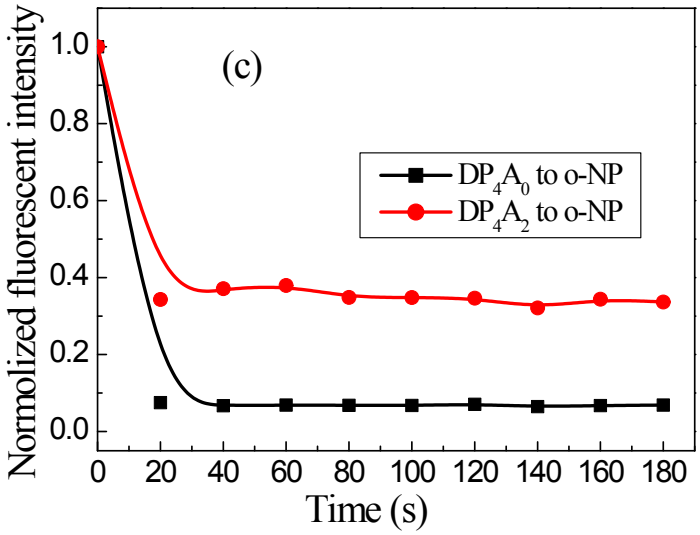

Fig. S3 Normalized fluorescence intensity of the (a) DP_4A_0 and (b) DP_4A_2 upon addition of o-NP for different periods of time. (c) The plots of fluorescence maximum of DP_4A_0 and DP_4A_2 as the function of time (DP_4A_0 dispersed in THF, excited at 370 nm, DP_4A_2 dispersed in DOX, excited at 370 nm, [o-NP]=2.5×10^{-4} mol L^{-1}).

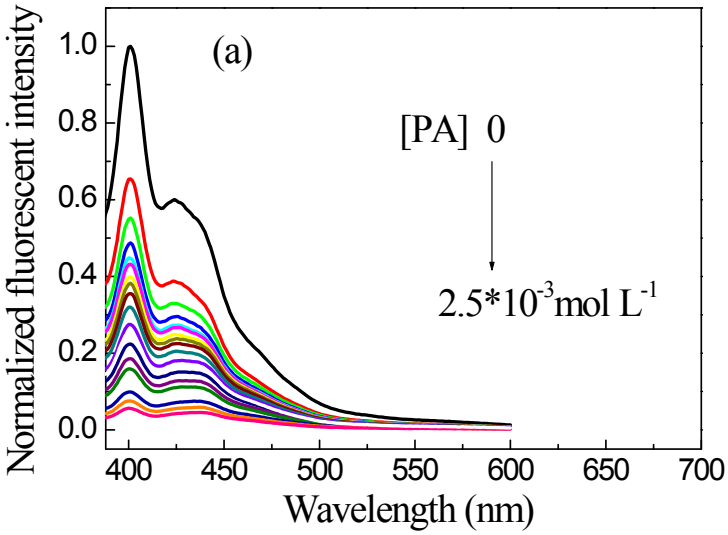
(a)
[PA] 0
2.5*10-3mol L-1
Normalized fluorescent intensity
Wavelength (nm)

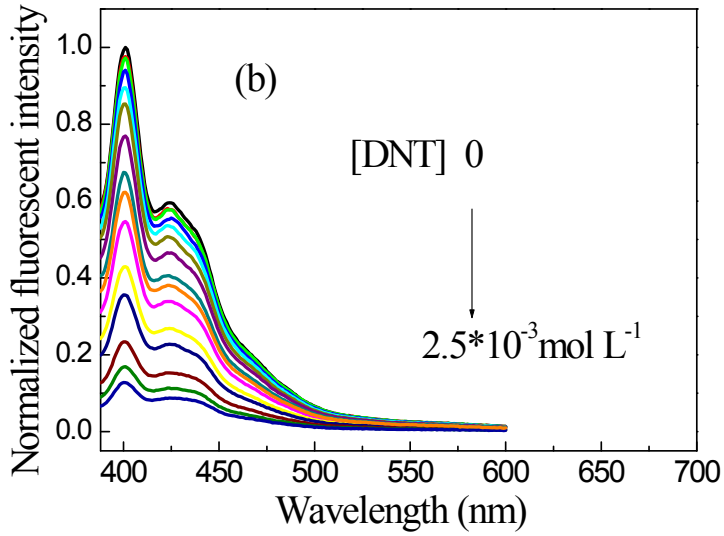
(b)
[DNT] 0
2.5*10-3mol L-1
Normalized fluorescent intensity
Wavelength (nm)

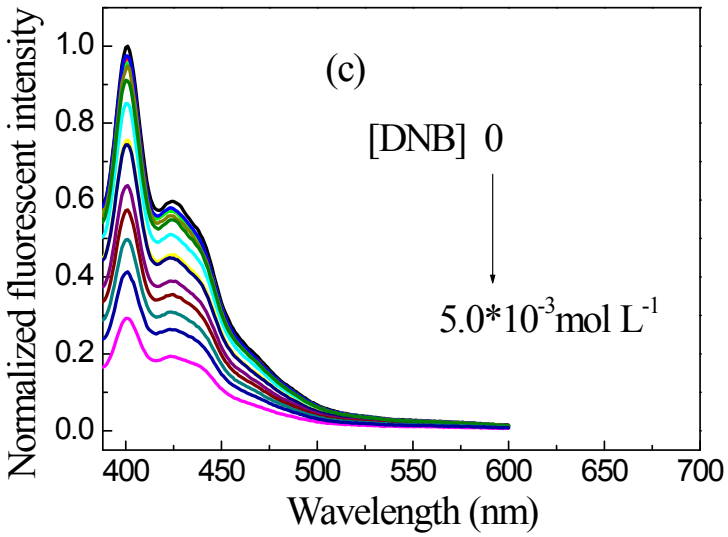
(c)
[DNB] 0
5.0*10-3mol L-1
Normalized fluorescent intensity
Wavelength (nm)

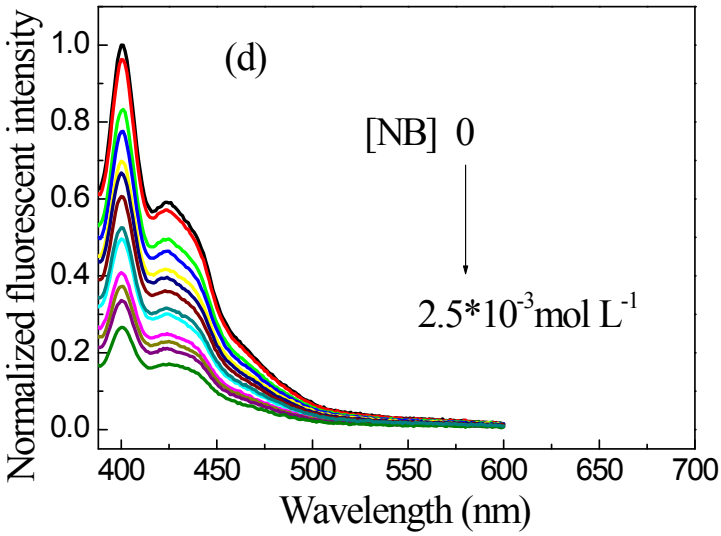
(d)
[NB] 0
2.5*10-3mol L-1
Normalized fluorescent intensity
Wavelength (nm)

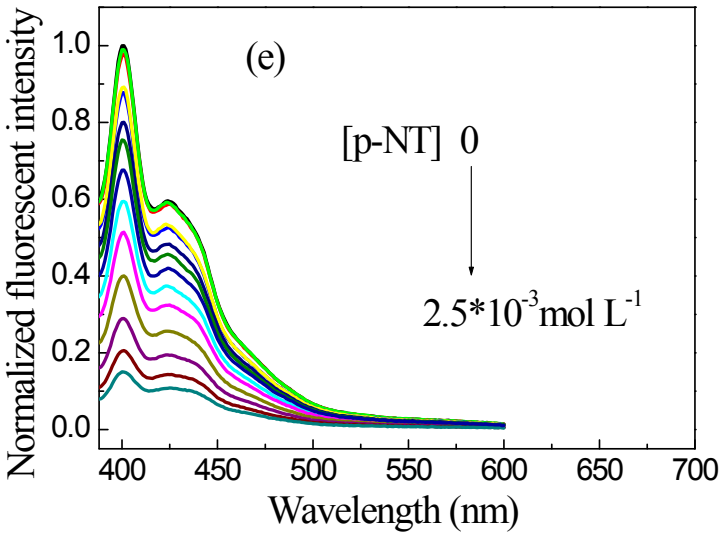
(e)
[p-NT] 0
2.5*10-3mol L-1
Normalized fluorescent intensity
Wavelength (nm)

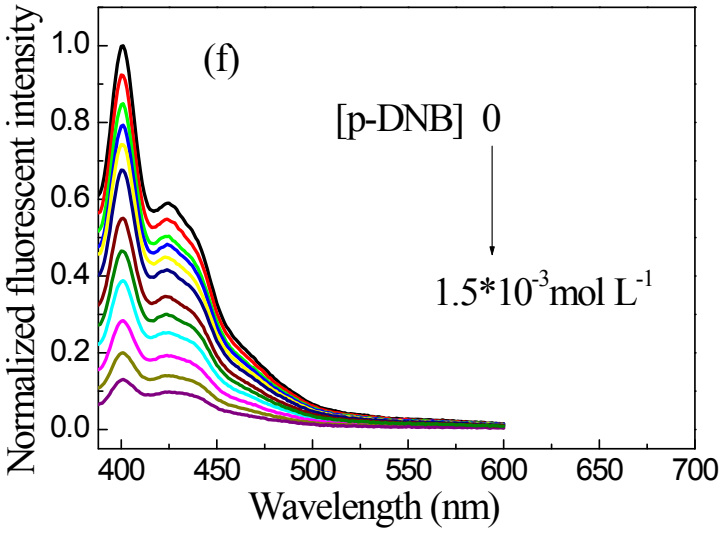
(f)
[p-DNB] 0
1.5*10-3mol L-1
Normalized fluorescent intensity
Wavelength (nm)

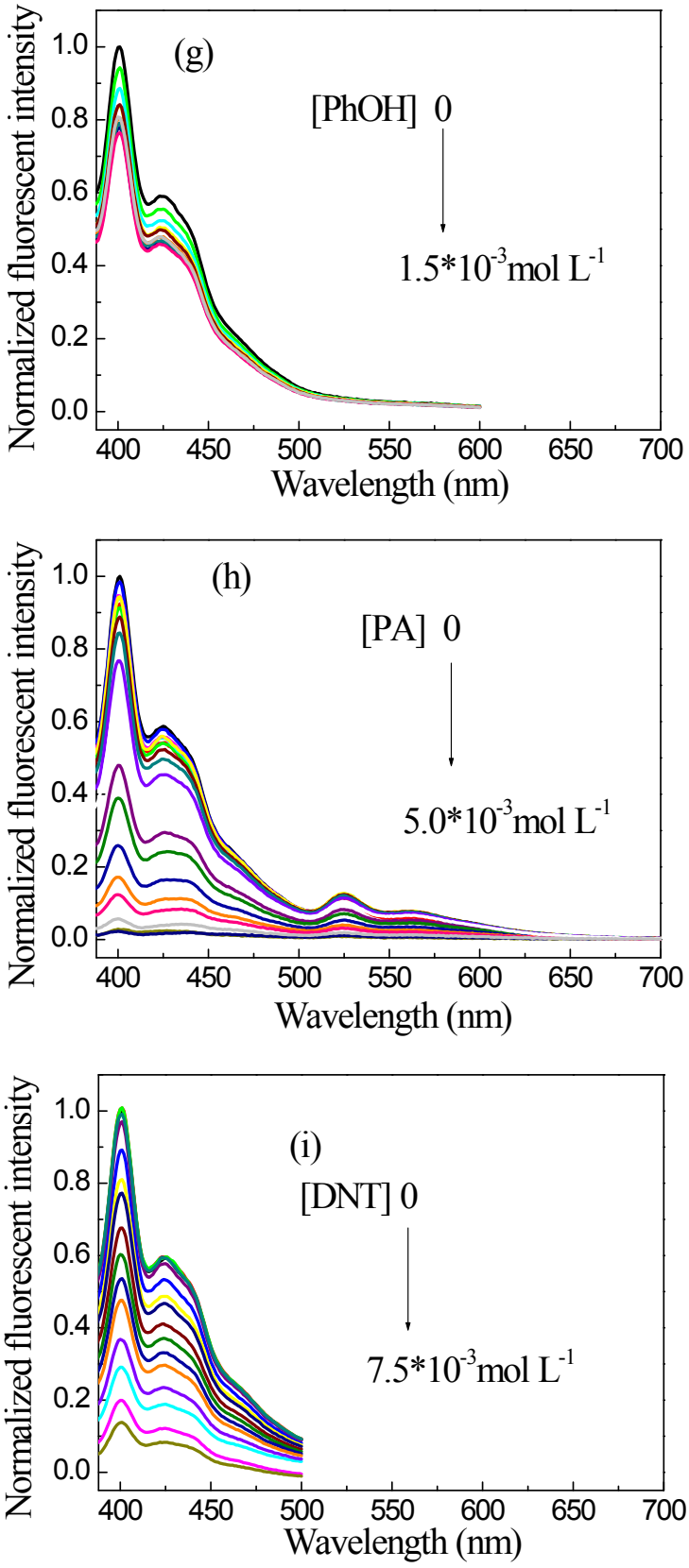
(g)
[PhOH] 0
1.5*10-3mol L-1
Normalized fluorescent intensity
Wavelength (nm)
(h)
[PA] 0
5.0*10-3mol L-1
Normalized fluorescent intensity
Wavelength (nm)
(i)
[DNT] 0
7.5*10-3mol L-1
Normalized fluorescent intensity
Wavelength (nm)

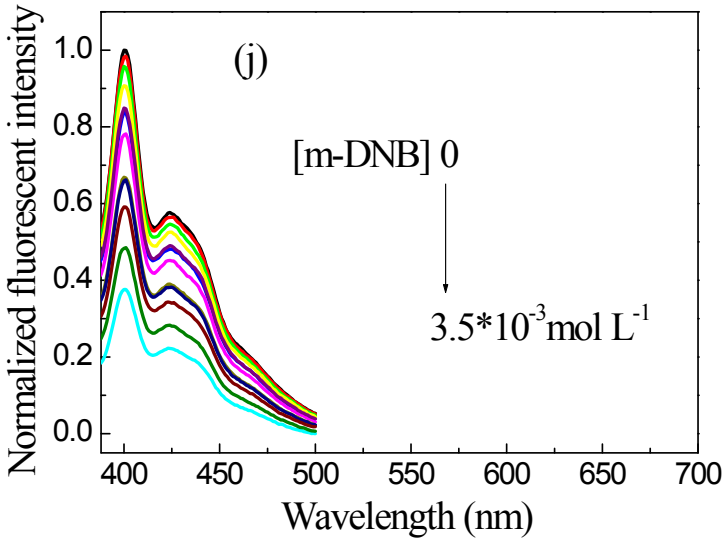
(j)
[m-DNB] 0
3.5*10-3mol L-1
Normalized fluorescent intensity
Wavelength (nm)
1.0
0.8
0.6
0.4
0.2
0.0
400
450
500
550
600
650
700

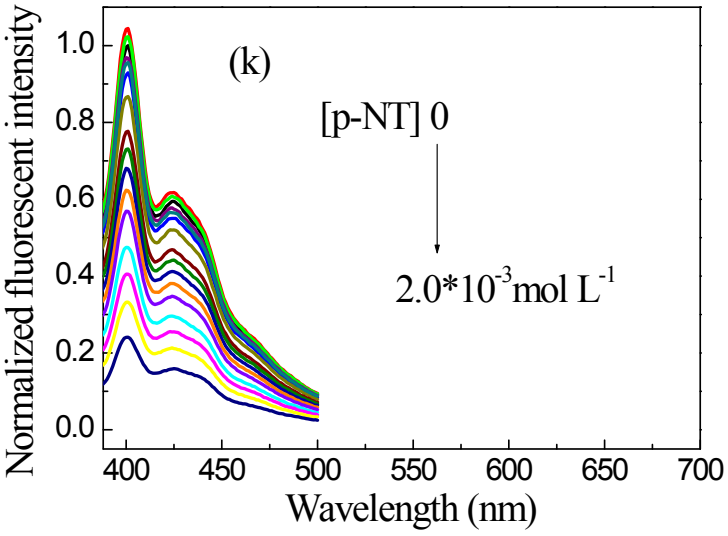
(k)
[p-NT] 0
2.0*10-3mol L-1
Normalized fluorescent intensity
Wavelength (nm)
1.0
0.8
0.6
0.4
0.2
0.0
400
450
500
550
600
650
700

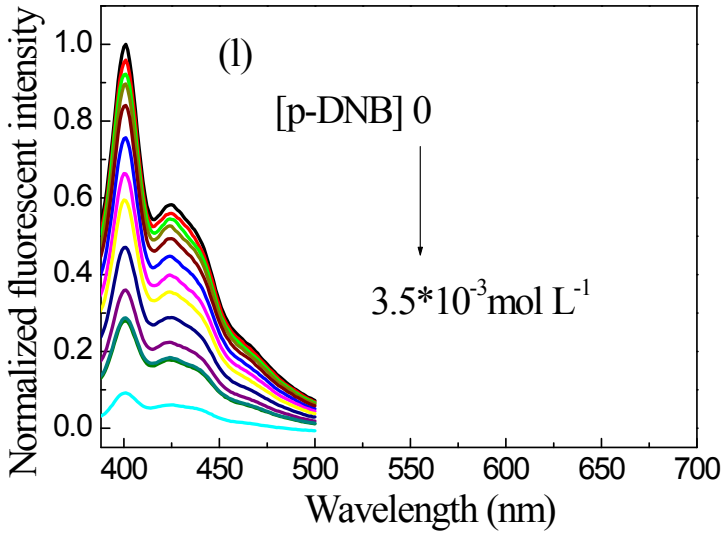
(l)
[p-DNB] 0
3.5*10-3mol L-1
Normalized fluorescent intensity
Wavelength (nm)
1.0
0.8
0.6
0.4
0.2
0.0
400
450
500
550
600
650
700

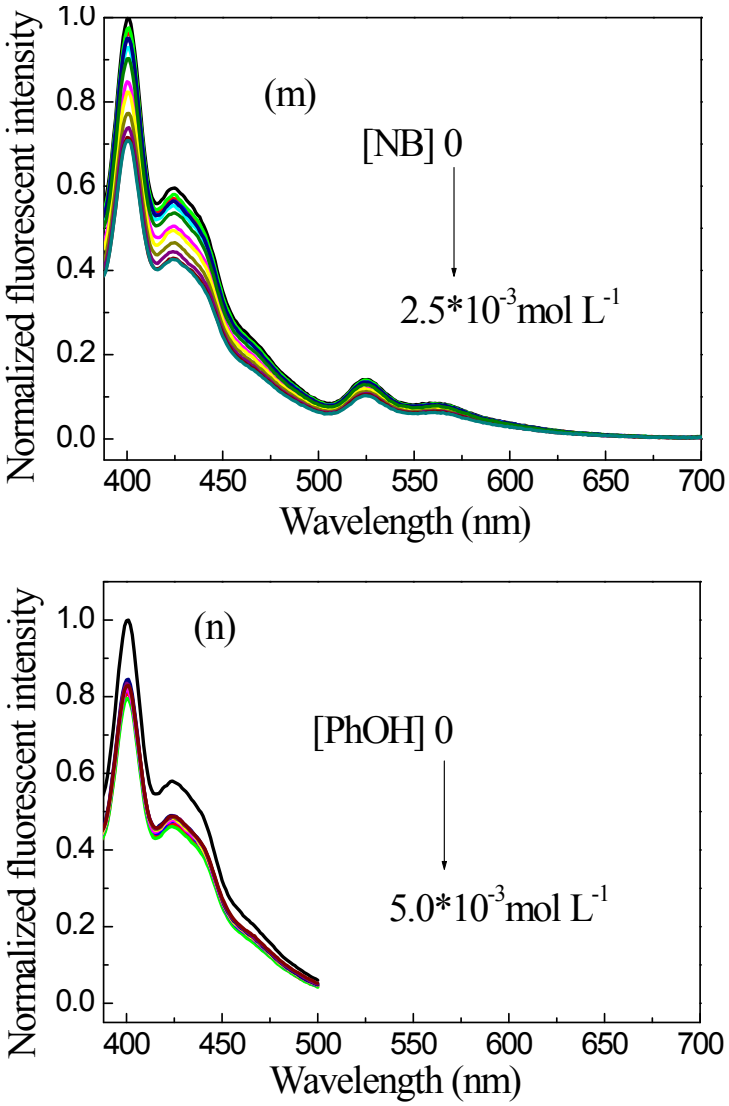

Fig. S4 The changes of fluorescence spectra of the (a)-(g) DP_4A_0 and (h)-(n) DP_4A_2 in dispersions of the THF and DOX upon addition of NACs (1.0 mg mL^{-1}, excited at 370 and 365 nm).

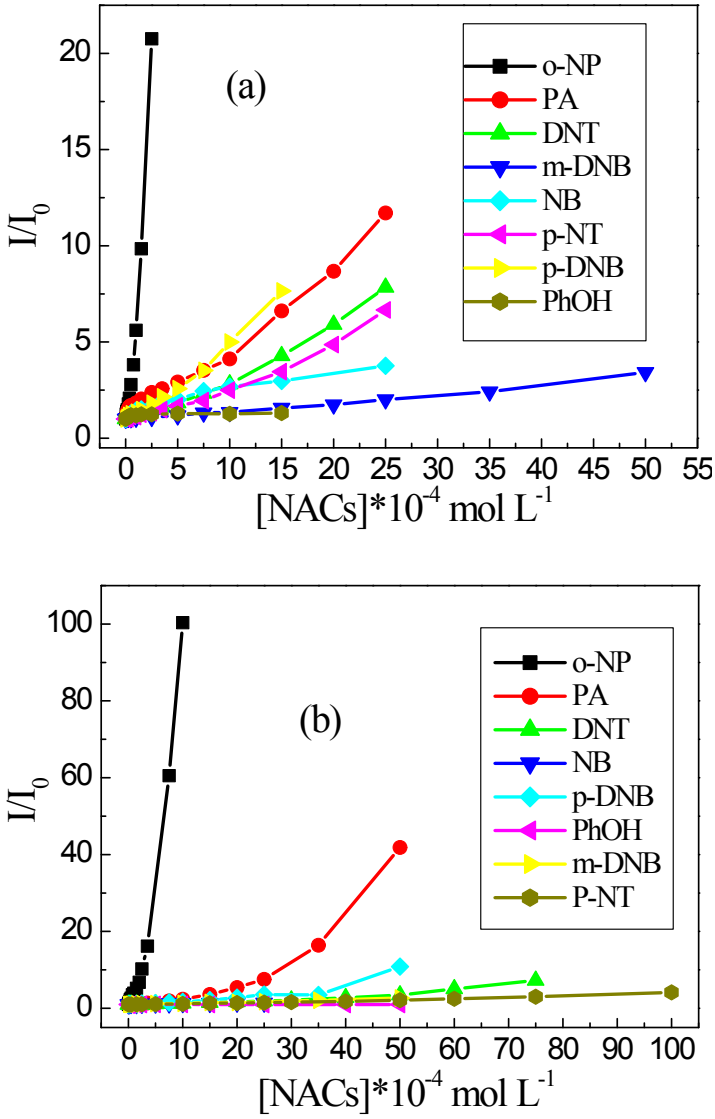

Fig. S5 Relative fluorescence intensity (I/I_0) of the (a) DP_4A_0 and (b) DP_4A_2 in suspensions upon addition of various concentrations of NACs (1.0 mg mL^{-1}, excited at 370 and 365 nm).

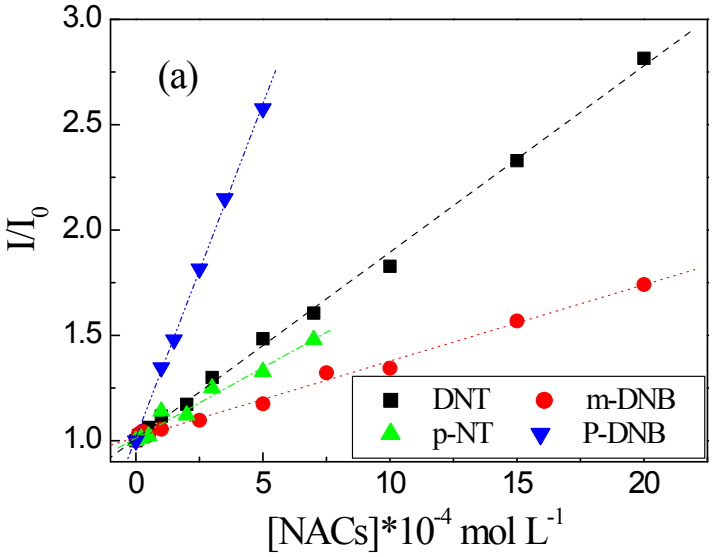
(a)
I/I0
[NACs]*10-4 mol L-1
DNT
m-DNB
p-NT
P-DNB

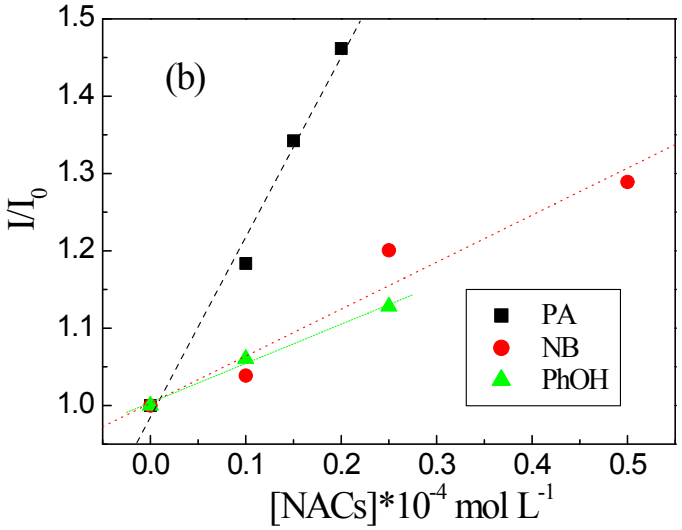
(b)
I/I0
[NACs]*10-4 mol L-1
PA
NB
PhOH

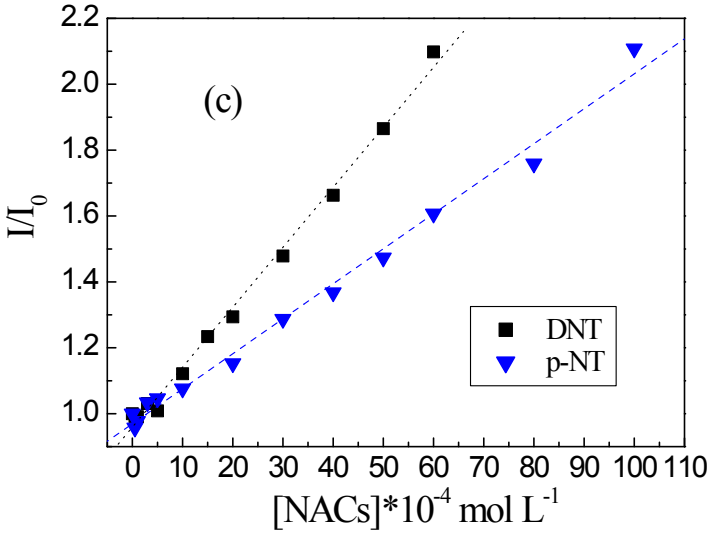
(c)
I/I0
[NACs]*10-4 mol L-1
DNT
p-NT

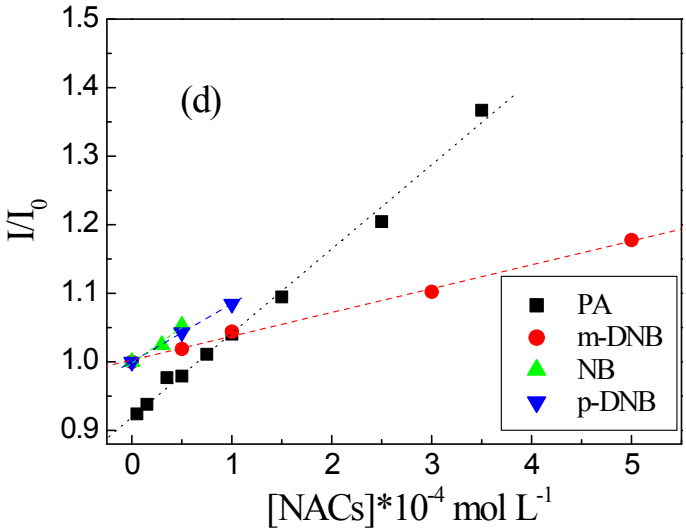

Fig. S6 Stern–Volmer plots of (a) (b) DP_4A_0 and (c) (d) DP_4A_2 with various concentrations of other NACs (1.0 mg mL^{-1}, excited at 370 and 365 nm).

Table S1 The equation of I_0/I of DP_4A_0 in THF (exciting at 370 nm) and DP_4A_2 in DOX (exciting at 365 nm) to the concentrations of other NACs for suspension.

CMPs	The equation	Regression coefficient (R)	The concentration range of NACs (mol L^{-1})	detection limit (mol L^{-1})
DP_2A_2	$I_0/I=1.0896+2.76\times10^4[PA]$	0.9994	5.0×10^{-6} to 2.5×10^{-5}	-
DP_4A_0	$I_0/I=0.9964+2.17\times10^4[PA]$	0.9918	0 to 2.5×10^{-5}	-
DP_4A_0	$I_0/I=1.0094+8.85\times10^2[DNT]$	0.9988	0 to 20×10^{-4}	-
DP_4A_0	$I_0/I=1.0151+3.62\times10^2$[m-DNB]	0.9968	0 to 20×10^{-4}	-
DP_4A_0	$I_0/I=1.0029+6.08\times10^3[NB]$	0.9721	0 to 0.5×10^{-4}	-
DP_4A_0	$I_0/I=1.0124+6.69\times10^3$[p-NT]	0.9831	0 to 7.0×10^{-4}	-
DP_4A_0	$I_0/I=1.0160+3.17\times10^3$[p-DNB]	0.9994	0 to 5.0×10^{-4}	-
DP_4A_0	$I_0/I=1.0036+5.03\times10^3$[PhOH]	0.9966	0 to 0.25×10^{-4}	-
DP_4A_2	$I_0/I=0.9190+1.23\times10^3[PA]$	0.9967	5.0×10^{-6} to 3.5×10^{-4}	-
DP_4A_2	$I_0/I=0.9590+1.82\times10^2[DNT]$	0.9971	0 to 60×10^{-4}	-
DP_4A_2	$I_0/I=1.0026+3.47\times10^2$[m-DNB]	0.9981	0 to 5×10^{-4}	-
DP_4A_2	$I_0/I=0.9982+1.04\times10^3[NB]$	0.9885	0 to 0.5×10^{-4}	-
DP_4A_2	$I_0/I=0.9694+1.06\times10^2$[p-NT]	0.9952	0 to 100×10^{-4}	-
DP_4A_2	$I_0/I=1.0002+8.45\times10^4$[p-DNB]	0.99997	0 to 1.0×10^{-4}	-

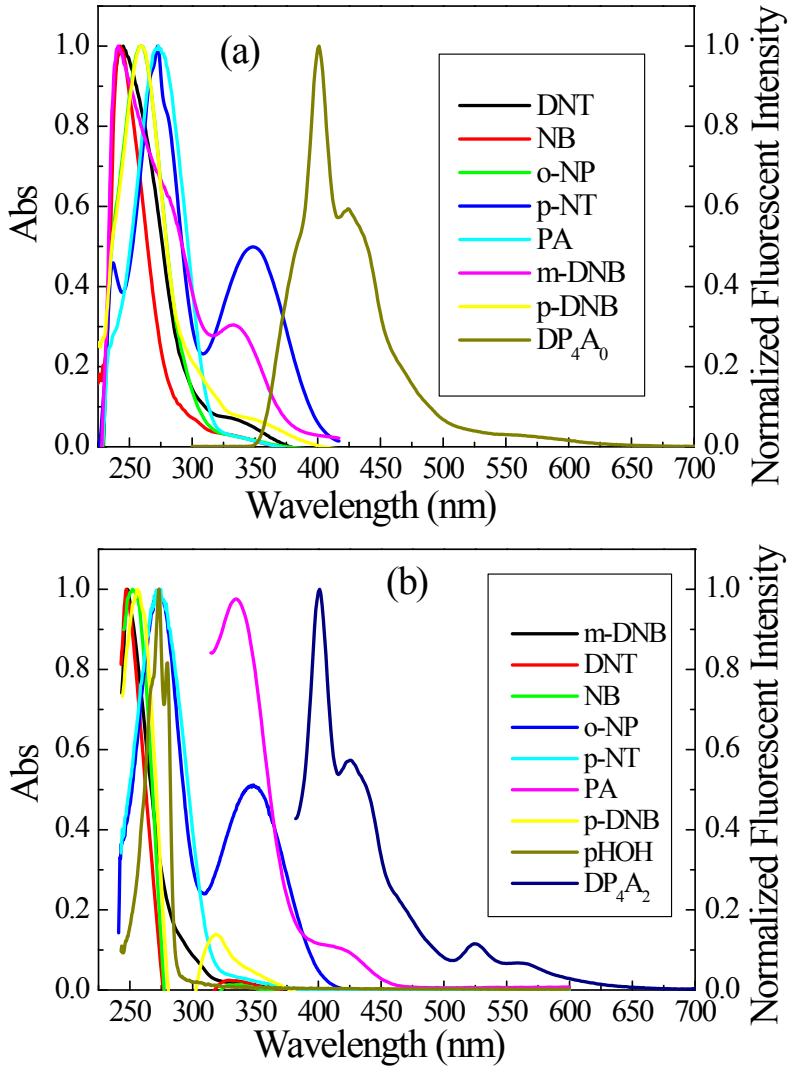

Fig. S7 Normalized of analyte absorption of and emission spectra of DP_4A_0 in THF (excitation wavelength: 370 nm) and DP_4A_2 in DOX (excitation wavelength: 365 nm).

Table S2 HOMO and LUMO calculations for CMPs and the NCAs. All the molecular orbital calculations were performed with the Gaussian 09 D. 01 program at the B3LYP/6-31G* level.

MO energy (eV)	DP_4A_0	DP_4A_2	o-NP	PA	p-DNB	m-DNB
LUMO	-3.291	-3.015	-2.711	-3.898	-3.495	-3.135
HOMO	-5.367	-5.688	-6.797	-8.237	-8.350	-8.413
MO energy (eV)	NB	DNT	p-NT	PhOH		
LUMO	-2.428	-2.977	-2.318	-0.3331		
HOMO	-7.591	-8.113	-7.364	-6.566		

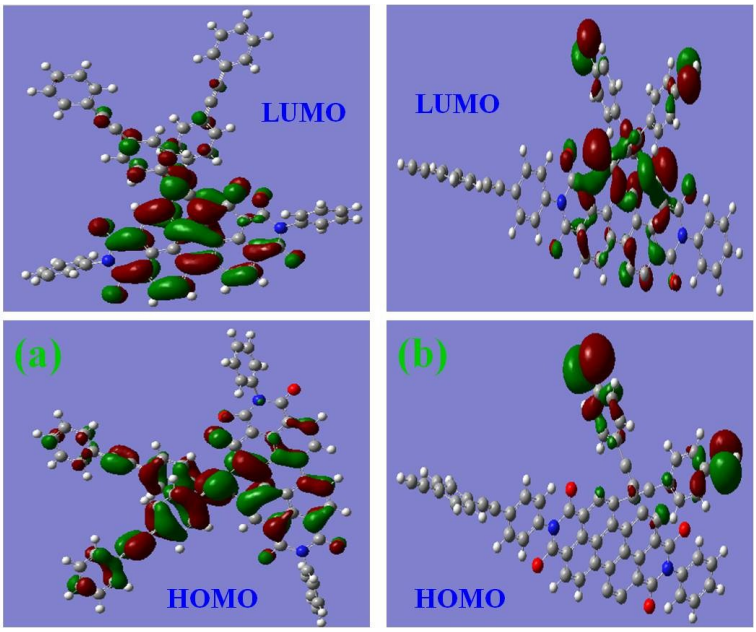

Fig. S8 HOMO and LUMO orbital diagrams of CMPs (a) DP_4A_0 and (b) DP_4A_2. The molecular orbital calculations were performed with the Gaussian 09 D. 01 program at the B3LYP/6-31G (d) level.

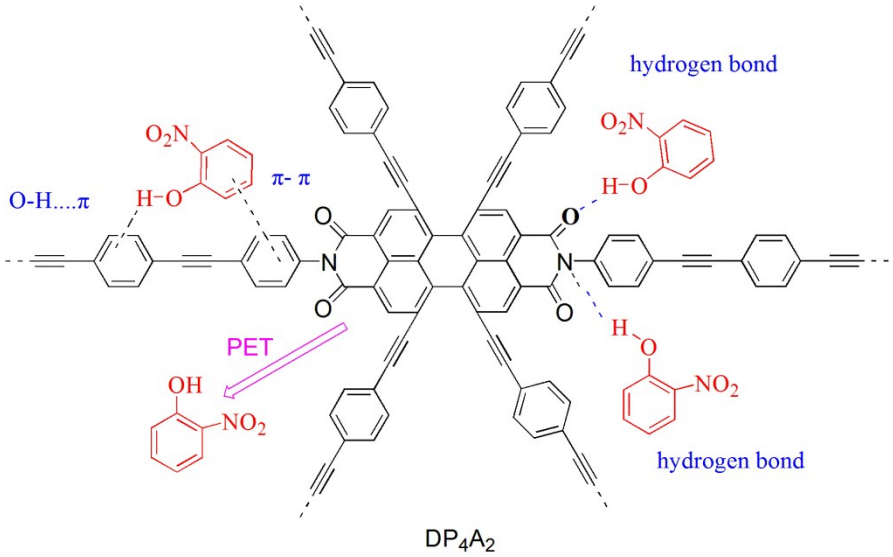

Fig. S9. Schematic image for the part of the 3-D network structure in DP_4A_2 interact with o-NP.

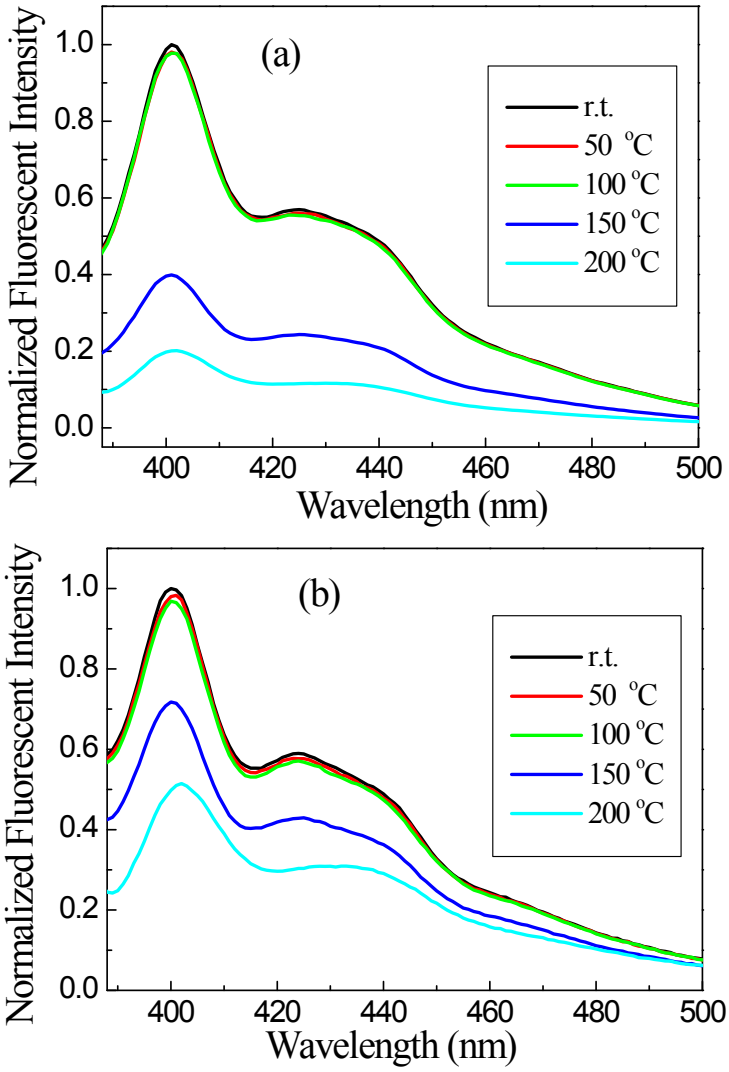

Fig. S10 Fluorescent spectra of dispersion of DP_4A_0 in THF (1.0 mg mL^{-1}, λex=370 nm) and DP_4A_0 in DOX (1.0 mg mL^{-1}, λex=370 nm), whose powders before and after baking at different temperatures for 30 min in air.